Romanian Reports in Physics, Vol. 63, No. 2, P. 456–464, 2011

RELAXATION TIMES MAPPING USING MAGNETIC RESONANCE IMAGING

LAURA FANEA, SILVIU A. SFRANGEU

The Emergency Clinical County Hospital Cluj-Napoca, No. 3-5,
Clinicilor street, 400006 Cluj-Napoca, Romania
Email: laura_fanea@yahoo.com

Received June 8, 2010

Abstract. Magnetic Resonance Imaging (MRI) techniques have been used to determine the spin-lattice, T_1, and the spin-spin, T_2, relaxation times in three phantoms with compositions simulating the T_1 and T_2 values of human tissues. Some methods of analysis were used in order to obtain the relaxation time maps. It has been shown that reliable results can be also obtained by using approximating methods of interest for clinical applications.

Key words: MRI, relaxation times.

1. INTRODUCTION

Magnetic resonance imaging (MRI) methods are now frequently used for the analysis of the diseased tissue. The methods are based on the fact that the spin-lattice, T_1, and the spin-spin, T_2, relaxation times are different as compared to that of the normal tissue [1,2]. The signal-to-noise ratio and the image resolution in MRI experiments are determined by the T_1 and T_2 relaxation times [3]. Clinically, the MRI methods based on relaxation times are rarely used due to the very long acquisition time required to obtain accurate T_1 and T_2 maps of the tissue. Consequently, there are only a few studies performed particularly using the magnetic resonance spectroscopy technique in order to obtain the relaxation times in the human brain [4-9]. For example, we mention the theoretical analysis of methods for the quantification of the T_1 and T_2 values [3,10] and several MRI studies performed on animals [2,11-13]. Generally, these studies were performed using magnetic field strengths ranging from 4 to 11.7 *T*.

The above mentioned methods are of great importance in evidencing the diseased tissues and consequently are now rapidly developing. In this context, in the present paper, we analyse several MRI methods for mapping the relaxation times T_1 and T_2 for possible clinical applications in analyzing the diseased tissues.

Three phantoms were evaluated and selected in order to cover the T_1 and T_2 values characteristic for different regions of the central nervous system.

2. METHODS

The MRI images of three phantoms were acquired using a 1T MRI system (Signa LX&MR/i8.3, GE Milwaukee, WI, USA) and a single loop 3-inch surface coil for ocular imaging. The phantoms were selected so that they contain solutions with different T_1 and T_2 values, in the range of those characteristic for the human central nervous system. A cross section image is given in Fig.1 and their compositions is listed in the figure caption.

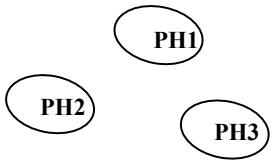

Fig.1 – The phantoms used for obtaining T_1 and T_2 maps. The phantoms are: PH1 (13 mM Gd in 0.9 % physiological saline); PH2 (26 mM Gd in 0.9 % physiological saline) and PH3 (0.9 % physiological saline). In all cases their volumes are 6 ml.

MRI images of the three phantoms were acquired using two pulse sequences. These images were processed to build T_1 and T_2 maps using different procedures, including an exact one (based on the fitting procedure) and two approximating the results of the above. The imaging parameters used for simulating human tissues are presented in Table1.

Table 1

Pulse sequences and imaging parameters used for MRI image acquisition

Pulse sequence	$T_R/T_E/T_I$*	Matrix	Voxel volume	Acquisition time
	ms/ms/ms	pixels x pixels	μm x μm x μm	min
fast spin echo	3000/10/-	256 x 128	78 x 78 x 2000	0.42
	3000/20/-	256 x 128	78 x 78 x 2000	0.42
	3000/40/-	256 x 128	78 x 78 x 2000	0.42
	3000/70/-	256 x 128	78 x 78 x 2000	0.42
	3000/100/-	256 x 128	78 x 78 x 2000	0.42
	3000/13.5/-	256 x 128	78 x 78 x 2000	0.42
	500/13.5/-	256 x 128	78 x 78 x 2000	0.42
inversion recovery spin echo	7000/11.1/50	256 x 128	78 x 78 x 2000	3.51
	7000/11.1/700	256 x 128	78 x 78 x 2000	3.51
	7000/11.1/1000	256 x 128	78 x 78 x 2000	3.51
	7000/11.1/2000	256 x 128	78 x 78 x 2000	3.51
	7000/11.1/4000	256 x 128	78 x 78 x 2000	3.51

* T_R = the repetition time; T_E = the echo time; T_I = the inversion time

The images obtained were used to construct the T_1 and T_2 maps using the inversion recovery and the fast spin echo pulse sequences, respectively. The inversion time, T_I, values during the image acquisition with the inversion recovery pulse sequence and the echo time, T_E, using the fast spin echo pulse sequence are given in Table 1. The analysed regions correspond to 256 × 128 pixels.

In order to obtain the exact solutions for constructing T_1 and T_2 maps, the signal intensity, SI, for each pixel were fitted with the relations [3,10,14,15]:

$$\mathrm{SI} = SI_0(1 - 2\exp(-T_I / T_1)), \tag{1}$$

$$\mathrm{SI} = SI_0(\exp(-T_E / T_2)). \tag{2}$$

SI_0 represents the intensity of the MRI signal corresponding to the proton system in the water pool at equilibrium.

The fitting procedure, in order to obtain T_1 and T_2 maps, was about 1h.

A proton density (PD), a T_1 weighted, T1w, and a T_2 weighted, T2w, fast spin echo pulse sequence were used to acquire in each case two sets of MRI images. The corresponding values for obtaining T_1 maps were T_R/T_E: 3 000/10 ms and 500/13.5 ms and for T_2 maps, T_R/T_E = 3 000/13.5 ms and 3 000/100 ms, respectively. The above sets of images were also processed to extract the T_1 and T_2 maps starting from relations which describe in an approximated way their evolution [14,15]:

$$T_1 = \frac{T_R}{\ln\left(1 - \dfrac{\mathrm{SI}(T1w)}{SI(PD)}\right)}, \tag{3}$$

$$T_2 = -\frac{T_E}{\ln\left(\dfrac{\mathrm{SI}(T2w)}{\mathrm{SI}(PD)}\right)}. \tag{4}$$

As a result of the above simplified relations, the image processing time was rather short, of few seconds.

The third method for T_2 estimation requires acquisition of two MRI images using the fast spin echo pulse sequence with two T_E values, namely T_{E1} = 10 ms and T_{E2} = 100 ms. In this case the spin-spin relaxation times were obtained using the relation [15]:

$$T_2 = \frac{T_{E2} - T_{E1}}{\ln \dfrac{\mathrm{SI}_1}{\mathrm{SI}_2}} \tag{5}$$

By SI_1 and SI_2 we denoted the intensity of the MRI signal corresponding to T_{E1} and T_{E2} values.

As above, the image processing involved only a few seconds.

The MRI images were read using the software MRIcro and processed using Matlab. In this program, the dicom MRI images, zero filled, were transformed in 256 × 256 matrices and each pixel for various slices was processed in order to obtain T_1 and T_2 maps, as above described. The matrices were then saved in dicom format and the mean T_1 and T_2 values, as well as their standard deviations, were measured using the software MIPAV. Finally, the obtained data were analysed in order to evaluate the accuracy of the different methods.

3. RESULTS

The T_1 map for one slice along with the five images used for the fitting procedure are given in Fig. 2. The minimum T_1 value was 64 ms (for the 26 mM Gd phantom) and the maximum T_1 was 2013 ms for the physiological saline phantom.

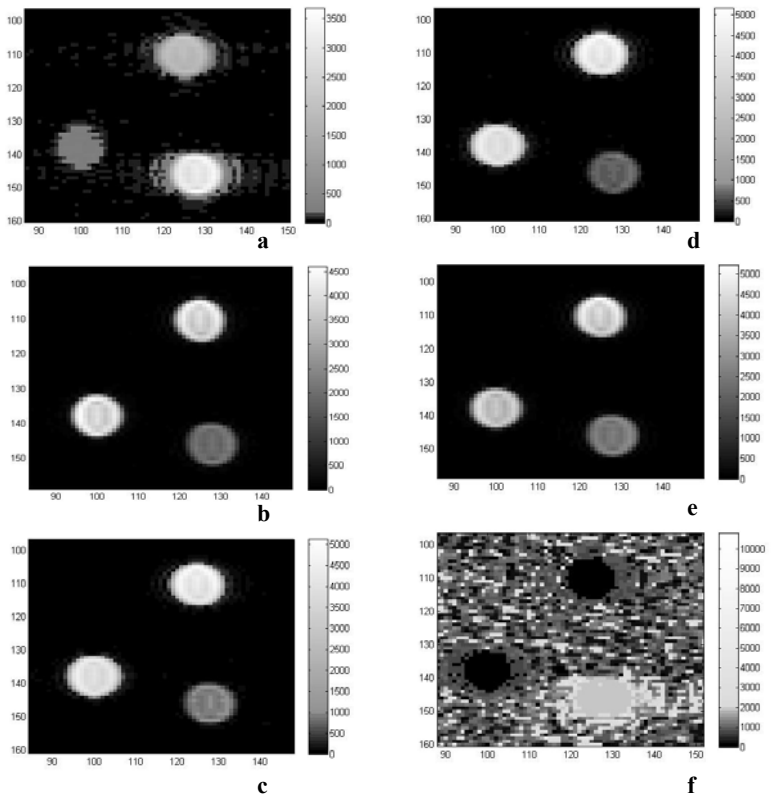

Fig. 2 – MRI images of the three phantoms acquired using the inversion recovery spin echo pulse sequence for T_1 values: a) 50 ms; b) 700 ms; c) 1 000 ms; d) 2 000 ms; e) 4 000 ms; f) T_1 map resulted after the fitting procedure.

The proton density MRI (a) and the T1w MRI (b) images obtained using the fast spin echo pulse sequence as well as the corresponding T_1 map is shown in Fig. 3. The minimum T_1 value obtained using this procedure was 69 ms for the phantom containing a 26 mM Gd concentration in physiological saline and the maximum relaxation time, 2 122 ms, was obtained for the phantom containing the 0.9 % physiological saline.

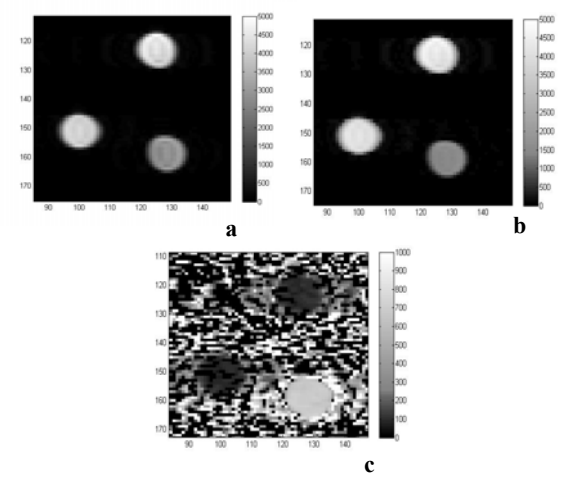

Fig. 3 – The proton density MRI (a) and the T1w MRI images (b) acquired using the fast spin echo pulse sequence as well as the corresponding T_1 map (c).

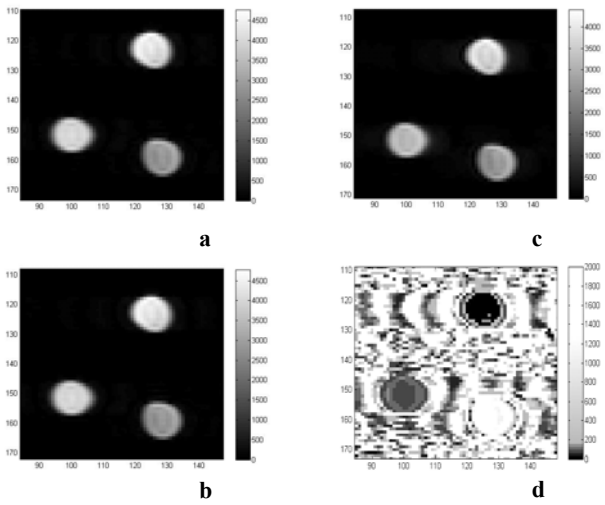

Fig. 4 – MRI images of the three phantoms acquired using the fast spin echo pulse sequence corresponding to T_E values of 10 ms (a), 20 ms (b) and 40 ms (c) and the T_2 map (d) resulted after the fitting procedure.

The T_2 map for one slice, along with the three of the five images used for the fitting procedure are given in Fig. 4. The minimum and maximum T_2 values were 72 ms for the phantom containing 26 mM Gd and 2 008 ms for the 0.9 % physiological saline phantom, respectively.

The T_2 maps of the phantoms imaged using the fast spin echo pulse sequence, obtained using equations (4) and (5) are given in Fig. 5 along with the T2w and the proton density images.

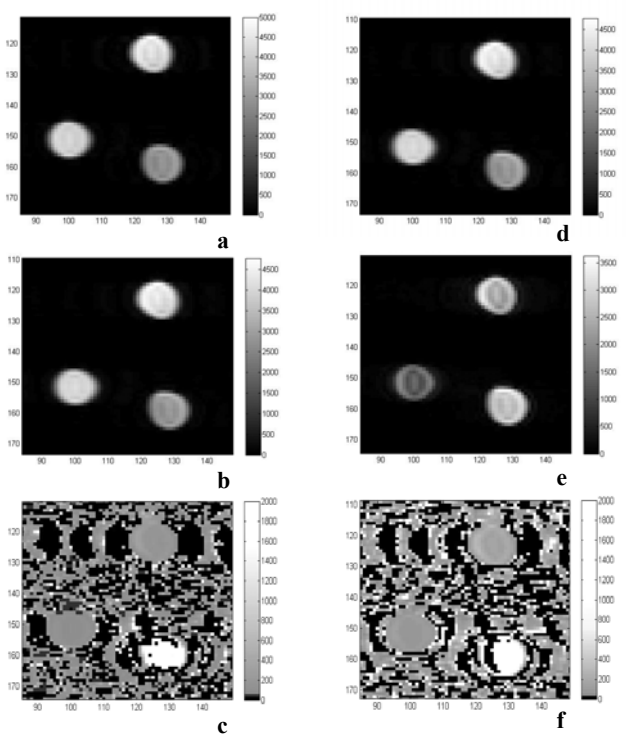

Fig. 5 – The proton density MRI image (a), the T2w MRI image (b) acquired using the fast spin echo pulse sequence and the corresponding T_2 map (c) obtained using relation (4). The MRI images acquired using the fast spin echo pulse sequence for T_Es of 10 ms (d) and 100 ms (e) and (f) the T_2 map obtained using equation (5).

The T_1 and T_2 values in the region of three phantoms were compared using the test. Mean values and standard deviations are given in Figs. 6 and 7. The differences of the mean values measured using different methods was assessed by calculating the probabilities, p. The T_1 values for phantom PH1 are not statistically different, they become somewhat different for phantom PH2 (*) and significantly different for phantom PH3 (***) – Fig.6. The mean T_2 values, in agreement with selected composition, calculated using the three methods are different for each phantom as seen in Fig. 7.

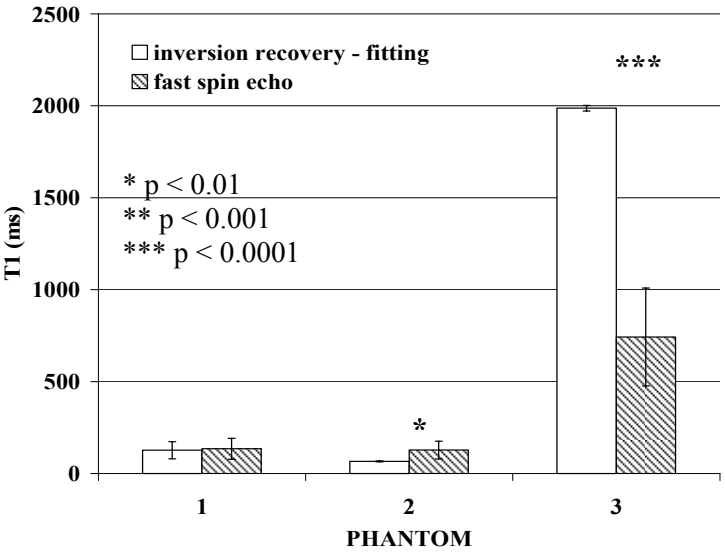

Fig. 6 – Mean T_1 values and the standard deviations for the three phantoms obtained using the inversion recovery and the fast spin echo pulse sequences.

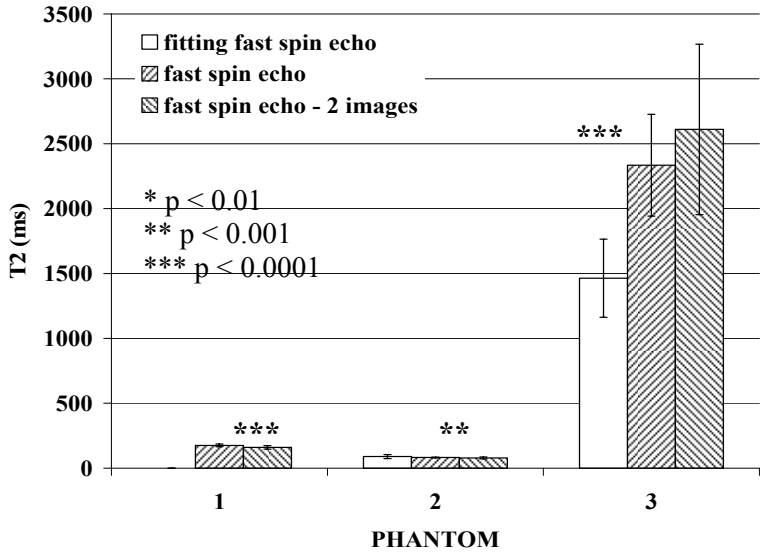

Fig. 7 – Mean T_2 values and the standard deviations in the region of three phantoms obtained using the fast spin echo pulse sequence, a fitting procedure and two image analysis, respectively.

4. DISCUSSION

Two methods, which give exact and approximate, respectively solutions, for the quantitative assessment of T_1 maps were studied. In the first method, the T_1 values were obtained by fitting the signal intensities of each pixel in five images acquired using the inversion recovery spin echo pulse sequence. The above T_1 values were compared to the corresponding ones obtained by acquiring a proton density and a T_1 weighted MRI image. The mean spin-lattice relaxation time determined by the above methods in the case of the first phantom are little different but they become somewhat different for the second and the third phantoms. The first method fits the data nonlinearly, while the second method approximates the signal intensity equations of the images. Although the exact method is assumed to give better results, the time consuming is rather long and consequently in clinical analyses the second method should be preferred. It is to be noted that the T_1 values estimated for the three phantoms cover the characteristic values of the central nervous system tissues.

Three other methods were used for the quantitative assessment of the spin-spin relaxation time. The first method estimates the T_2 values by fitting the signal intensities of each pixel in five MRI images acquired using the fast spin echo pulse sequence. The T_2 values were then compared to those obtained by acquiring a proton density and a T_2 weighted MRI image. The T_2 values for each pixel were also estimated using two images acquired using the fast spin echo pulse sequence with two different T_E values. Nonlinear fitting procedure, as in case of spin-lattice relaxation time, T_1 is time consuming, while the second method makes approximations on the signal intensity analyses. The T_2 values estimated using these three methods were not significantly different in the case of the phantom 2 (method 1 compared against method 2) and for phantom 3 (method 2 compared with method 3). As in case of spin-lattice relaxation time, the T_2 values ($70 \leq T_2 \leq 3782$ ms) cover those of the tissues in the central nervous system and, they have, therefore, clinical potential applications.

As a conclusion, methods of analyses of relaxation times using MRI techniques with potential clinical applications were suggested. The analyses based on approximate solutions require rather short time of processing the data and give results close to those obtained using an exact method of analysis.

REFERENCES

1. R.V. Damadian, Science, **171**, 1151–1153 (1971).
2. R.A. de Graaf, P.B. Brown, S. McIntyre, T.W. Nixon, K.L. Behar, D.L. Rothman, Magn. Reson. Med., **56**, 386–394 (2006).
3. R. I. Shrager, G. H. Weiss, R. G. S. Spence. NMR Biomed., **11,** 297–305 (1998).
4. C.G. Choi, J. Frahm, Magn. Reson. Med., **41**, 204–207 (1999).

5. J. Frahm, H. Bruhn, M.L. Gyngell, K.D. Merboldt, W. Hanicke, R. Sauter, Magn. Reson. Med., **11**, 47–63 (1989).
6. O. Henriksen, NMR Biomed., **8**, 139–148 (1995).
7. H.P. Hetherington, G.F. Mason, J.W. Pan, S.L. Ponder, J.T. Vaughan, D.B. Tweig, G.M. pohost, Magn. Reson. Med., **32**, 565–571(1994).
8. V. Mlynarik, S. Gruber, E. Moser, NMR Biomed., **14**, 325–331 (2001).
9. S. Posse, C.A. Cuenod, R. Risinger, D. Le Bihan, R.S. Balaban, Magn. Reson. Med., **33**,246–252 (1995).
10. P.B. Kingsley, Concepts in Magn. Reson., **11**, 29–49 (1999).
11. J. Chen, Q. Wang, H. Zhang, X. Yang, J. Wang, B.A. Berkowitz, S.A. Wickline, S.K. Song, Magn. Reson. Med., **59**, 731–738 (2008).
12. Q. Shen, H. Cheng, M.T. Pardue, T.F. Chang, G. Nair, V.T. Vo, R.D. Shonat, T.Q. Duong, J. Magn. Reson. Imaging., **23**, 65–472 (2006).
13. G. Nair, Q. Shen, T.Q. Duong, Neuroimaging., **20**, 126–130 (2010).
14. E.M. Haacke, R.W. Brown, M.R. *Thompson, R. Venkatesan, Magnetic Resonance Imaging: Physical Principles and Sequence Design*, John Wiley & Sons Inc., USA. 129–133 (1999).
15. E.M. Haacke, R.W. Brown, M.R. Thompson, R. Venkatesan, *Magnetic Resonance Imaging: Physical Principles and Sequence Design*, John Wiley & Sons Inc., USA. 118–123 (1999).